Eur. Phys. J. B **45**, 249–260 (2005)
DOI: 10.1140/epjb/e2005-00056-0

THE EUROPEAN
PHYSICAL JOURNAL B

Nonuniform and sequential magnetization reversal via domain structure formation for multilayered system with grain size induced enhanced exchange bias

A. Paul[a], E. Kentzinger, U. Rücker, D.E. Bürgler, and P. Grünberg

Institut für Festkörperforschung, Forschungszentrum Jülich GmbH, 52425 Jülich, Germany

Received 13 September 2004
Published online 8 March 2005 – © EDP Sciences, Società Italiana di Fisica, Springer-Verlag 2005

Abstract. We report on the magnetization reversal in series of exchange-biased multilayers NiFe(10.0 nm)/[$Ir_{20}Mn_{80}$(6.0 nm)/$Co_{80}Fe_{20}$(3.0 nm)]$_N$ studied by specular reflection and off-specular scattering of polarized neutrons. All specimens are sputtered and post-annealed at 530 K (i.e. above the IrMn Néel temperature of 520 K) in Ar atmosphere before cooling to room temperature in the presence of a field of 130 Oe which induces the unidirectional anisotropy. We find H_{EB} is dependent upon the number of bilayers N as it gradually increases from 0.33 kOe for $N = 1$ to a considerably higher value of upto $\approx$0.9 kOe for $N = 10$. X-ray specular and diffuse scattering data reveal no significant variation of the lateral correlation length and only a weak dependence of the vertical rms interface roughness on N. Atomic and magnetic force microscopy, however, show a strong reduction of the grain size accompanied by distinct changes of the ferromagnetic domain structure. The enhancement of the exchange bias effect is presumably related to the shrinking of the related domain size in the antiferromagnet due to the structural evolution in the multilayers. Polarized neutron reflectometry (PNR) measurements are done at different applied fields sweeping both branches of the hysteresis loop. The spin-flip (SF) cross section of both the $N = 10$ and 3 samples show diffusely scattered intensity appears gradually as the field approaches H_{EB} and is most intense where the net magnetization vanishes. The disappearance of diffuse scattering in saturation indicates that the off-specular intensity is related to the reversal process. The reversal proceeds sequentially starting with the bottom (top) CoFe layer for decreasing (increasing) field and is related to the evolution of the grain size along the stack. The reversal of each CoFe layer is for both field branches due to domain wall motion. Thus as a main result, we observe a sequential and symmetric magnetization reversal in exchange-biased multilayers. The concomitant in-plane magnetization fluctuations revealed by off-specular spin-flip scattering indicate a more complex reversal mechanism than hitherto considered. Moreover, although the grain size decreases from $N = 3$ to 10 by a factor of about four the reversal mechanism remains similar.

PACS. 75.70.Cn Magnetic properties of interfaces (multilayers, superlattices, heterostructures) – 75.60.Jk Magnetization reversal mechanisms – 61.12.Ha Neutron reflectometry

1 Introduction

When a ferromagnet (FM)/antiferromagnetic (AF) bilayer is cooled below its blocking temperature in an external field H_{FC} [1], a direct exchange coupling between FM and AF layers results in the shift of the hysteresis loop of the ferromagnetic layer (shift of the center from the zero field) along field axis which is termed as the exchange bias [2]. Consequently, the hysteresis loop of the FM layer is usually shifted to negative fields. However though the "locking" of the magnetization is not fully understood yet the spin-valve structures have attracted much interest due to its potential usage as magnetoresistive sensors [3] and, thus, has recently attracted intense attention (for reviews see [4]).

From the very first observation of exchange bias in reference [2] asymmetric hysteresis loops due to asymmetric magnetization reversal processes are being observed in many experiments [5–9]. The asymmetry is considered for increasing/decreasing applied field H_a for the hysteresis loop with respect to the filed cooling direction H_{FC}. The underlying mechanism is expected to have crucial importance to elucidate the exchange bias effect. In response to an applied external field sweeping, the net magnetization M undergoes a reversal as the condition $\overrightarrow{M} \cdot \overrightarrow{H_a} = 0$ is satisfied. This can be realized in two ways; either by undergoing a condition where the net magnetization is zero or alternatively, when the net magnetization (without any change in magnitude) rotate, yielding a maximum for the component $M_\perp$. Recently, asymmetric magnetization reversal processes of Fe films exchange-biased by twinned

---

[a] e-mail: `a.paul@fz-juelich.de`

MnF_2 and FeF_2 AF layers [7] and Co/CoO bilayers [8,9] have been examined by polarized neutron reflectometry (PNR).

Depth dependent vector magnetometry can be obtained by PNR measurements with polarization analysis [10]. When the component of the in-plane magnetic induction is parallel to the neutron spin (or the polarization i.e. the applied field direction) it do not change its spin eigenstate and are thus observed as non spin flip scattering (NSF). Whereas the components of the magnetization orthogonal to the neutron spin results in a change in potential which is purely magnetic and can flip the eigenstate of the incident neutron. This is referred to as the spin flip scattering (SF). In all the PNR experimental reports, reversal by magnetization rotation is identified by a significant increase of the specular reflectivities in the SF channels (R_{+-} and R_{-+}) which are exclusively of magnetic origin and correspond to magnetization components perpendicular to H_a which is also a guiding field provided for neutron polarization applied collinear to H_{FC}. Reversal by domain nucleation and propagation does not provide enhanced SF intensities, because the magnetization is always collinear to H_a and solely shows up in the specular NSF reflectivities (R_{++} and R_{--}) as an additional contribution to the non-magnetic reflectivity. In reference [7] it is argued that the unidirectional anisotropy hinders the formation of domains with magnetization antiparallel to the cooling field direction and favors magnetization rotation for the decreasing field branch [1]. However, when the field is increased domains with the magnetization parallel to H_{FC} are energetically favorable, and the remagnetization proceeds via domain nucleation and propagation. Just the opposite reversal mechanisms are reported for the Co/CoO system [8,9], where domain wall motion occurs for the decreasing field branch and magnetization rotation for increasing fields. Both systems are epitaxially grown, but the dependence on the direction of H_{FC} with respect to the twinning axes in reference [7] and training effects in reference [9] hamper a direct comparison.

Theoretically the interpretation of the magnetization reversal was discussed in reference [11]. This is governed by an effective field H_{eff} arising from the anisotropy of the FM, the exchange bias field of the AF, and the applied field H_a. H_{eff} and the torque it exerts on the FM magnetization depend on the angle θ between H_a and the AF anisotropy axis. Beckmann et al. show that depending on θ the reversal mode is either by coherent rotation for both loop branches or asymmetric with a nonuniform reversal for the increasing branch. Here nonuniform refer to the reversal of magnetization with no component perpendicular to the H_a direction. However a reversal mode which is symmetric, but nonuniform corresponds to the situation where $\theta = 0$, i.e. for no misalignment between the exchange bias axis and the applied field.

In the present work, we investigate the evolution of the layer-by-layer magnetization configuration of polycrystalline $[Ir_{20}Mn_{80}/Co_{80}Fe_{20}]_N$ multilayers (MLs) along a full magnetization loop by specular and off-specular PNR. In our experiment, the condition $\theta = 0$ is fulfilled as there is no experimental deviation between the field-cooling axis and the axis of the field applied for the remagnetization experiments. On the other hand, our polycrystalline multilayer samples may give rise to a more complex behavior than modeled in reference [11]. The microstructure reveals structural evolution of cluster sizes and shrinking of FM domains with number of bilayers. We find sequential switching of the layers that we relate to the microstructural evolution along the stack. Here we also address the influence of a granular structure by comparing the magnetization reversal of exchange-biased samples with different grain sizes i.e. MLs with different N. The reversal proceeds for both loop branches by domain wall motion, but is accompanied by fluctuations of the in-plane magnetization component perpendicular to H_a. We find no indication of coherent rotation of the magnetization in our samples.

2 Experiment

The exchanged bias spin-valves studied in the present work are multilayer (ML) structures of $[Ir_{20}\ Mn_{80}(6.0\ nm)/Co_{80}Fe_{20}(3.0\ nm)] \times N$ prepared by dc magnetron sputtering, where N is the number of bilayers. A base pressure of 5×10^{-8} mbar is achieved by turbo-molecular pumps. We employ a 10 nm-thick NiFe buffer layer grown on oxidized Si wafers in order to improve the texture of the MLs. All specimens are first annealed at 533 K, i.e. above the Néel temperature $T_N = 520$ K of IrMn, for 60 minutes in Ar gas and then cooled to room temperature (RT) in an external field of 130 Oe in order to induce the unidirectional anisotropy. Data concerning magnetic properties is taken after several remagnetization cycles in order to exclude training effects.

The microstructure and the layer quality are investigated by low angle X-ray reflectivity (XRR) and X-ray diffuse scattering (XDS) measurements [12–14]. XRR and XDS measurements are done using a Bruker-axs D8 diffractometer with Cu-K_α radiation. We measured in specular geometry with the angle of incidence θ_i equal to the exit angle θ_f as well as in off-specular geometry with an offset of $\Delta\omega = 0.13$ degree between θ_i and θ_f. True specular reflectivity is obtained by subtracting the off-specularly scattered intensity from the specular one. Diffuse scattering as a function of the in-plane component of the momentum transfer vector, q_x, as measured by keeping the scattering angle 2θ fixed and rocking the specimen around $\theta_i = \theta_f$. The diffuse scattering measurement provides information about the structure of the interfaces in the film plane. The in-plane structure of the interfaces can be described in terms of a height-height correlation function, $c(x, y)$, which in most of the cases can be written as

$$C(x, y) = \sigma^2 \exp\left(-\left[\frac{|R|}{\xi}\right]^{2h}\right), \quad (1)$$

where $R = (x^2 + y^2)^{1/2}$, and ξ is the in-plane correlation length of the interface height variations and h is the

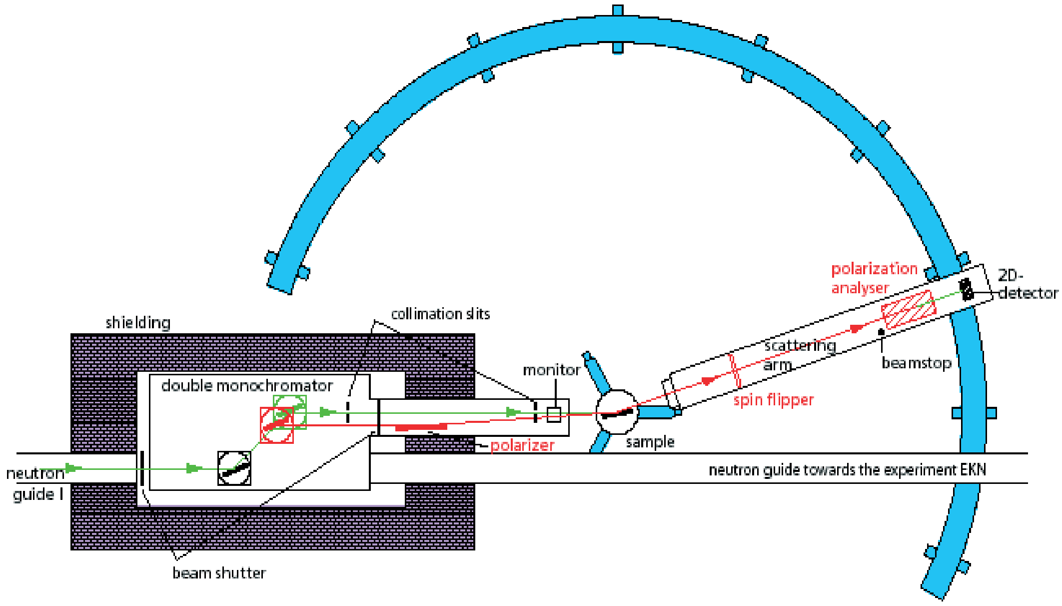

Fig. 1. The HADAS reflectometer at the Jülich research reactor FRJ-2 (DIDO). The unique feature of this instrument lies in its polarization analysis of the neutrons, allowing the simultaneous measurement of the spin direction scattered over the whole range of the 2D detector.

fractal dimension which takes care of jaggedness of the interface [14]. Magnetization loops are recorded by means of a superconducting quantum interference device (SQUID) as well as the magneto-optic Kerr effect (MOKE). Atomic and magnetic force microscopy (AFM/MFM) measurements in tapping mode are performed with a multimode SPM from Digital Instruments using Co-based magnetic tips.

PNR measurements are performed at the polarized neutron reflectometer with polarization analysis HADAS [15] at the Jülich research reactor FRJ-2 (DIDO). The neutron wavelength is fixed at $\lambda = 4.52$ Å. Figure 1 shows the experimental set-up for neutron scattering. The instrument is equipped with a 2D detector with a special spin analyzer. The horizontal position of the stacked analyzer supermirrors makes the horizontal component of the detected neutrons unchanged thus providing identical polarization conditions over the whole area of the detector and thus allows simultaneously measuring specular and off-specular intensities with polarization analysis. The polarization efficiencies of the polarizer and analyzer are 96% and 95%, respectively. The specimens are kept at RT and a guiding field H_a of up to 15 kOe can be applied. We perform layer-resolved magnetometry [16,17] by analyzing and fitting specular NSF and SF reflectivity cross sections. In specular geometry (angle of incidence α_i equal to the exit angle α_f), the reflectivities follow from energy and in-plane momentum conservation laws. Normal wave vector transfers $Q_\perp = \frac{2\pi}{\lambda}[\sin(\alpha_i) + \sin(\alpha_f)]$ are probed. Off-specular scattering arises when the in-plane translational symmetry is broken by interface roughness or magnetic domains on a length scale shorter than the in-plane projection $l_\| \approx 2\pi/\delta Q_\|$ of the coherence length of the neutron beam, where $\delta Q_\|$ is the uncertainty of the in-plane momentum transfer $Q_\| = \frac{2\pi}{\lambda}[\cos(\alpha_f) - \cos(\alpha_i)]$ [18]. For our instrument $l_\|$ exceeds 20 μm, but the resolution of the 2D detector defines an upper limit of about 20–30 μm for the resolvable lateral structure size. A lower limit of about 1 μm results from the limited neutron flux at the sample position.

3 Results

3.1 Magnetization measurements

Figure 2 shows the magnetic hysteresis loops as obtained from (a) SQUID and (b) MOKE measurements for different N. There are always two hysteresis loops, one corresponding to the magnetically soft (and interestingly enough always unpinned) NiFe buffer layer and the other to the pinned CoFe layer(s) in the ML. The relative contributions to the sample's total moment confirm this assignment. The averaging over an increasing number of CoFe layers results in slanted loops for larger N. The exchange bias field H_{EB} clearly increases form 330 Oe for $N = 1$ to about 900 Oe for $N = 10$, and it tends to saturate [Fig. 4c]. This is even more evident in the MOKE data, where the limited penetration depth of the laser light (about 20 nm) enhances the relative weight of the topmost CoFe layers.

3.2 X-ray measurements

Figure 3a shows the X-ray reflectivity scans of the multilayers along with their fit. Using the coherent scattering approximation developed by Parratt [19] the patterns are fitted by the least square method using the standard optical formalism according to Nevot and Croce [20] with the

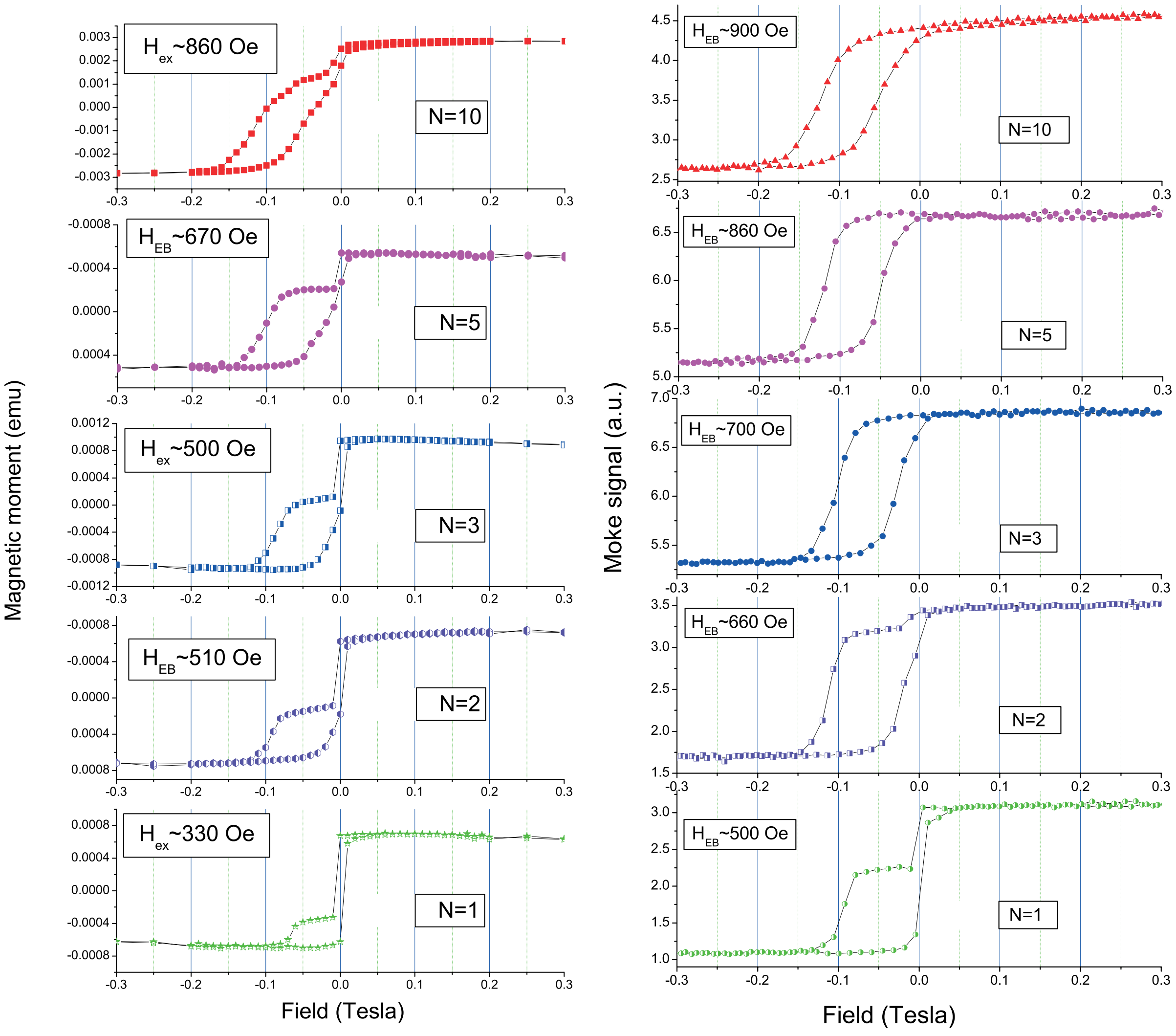

(a) (b)

Fig. 2. Magnetization loops of SiO$_2$/NiFe(10.0 nm)/[IrMn(6.0 nm)/CoFe(3.0 nm)] × N MLs with the number of bilayers N as measured by (a) SQUID and (b) MOKE.

following constraints: (i) The roughness of all IrMn/CoFe interfaces is assumed to be equal and is represented by a single fitting variable σ. (ii) The individual layer thicknesses are fitting parameters. (iii) The top Co layer is expected to be oxidized, and hence its electron density as well as its thickness are separate fitting parameters. We do not consider any intermixed layer due to the positive heat of mixing for the AF and FM layer. The values obtained from the fit are given alongside. The fits yield a rather weak increase of σ from 0.3 to 0.6 nm as N increases from 1 to 10. The evolution of σ of such order of magnitude is common for MLs [12,21] and largely depends on the state of the interfaces and the thermodynamics of the elements. The presence of Bragg peaks and total thickness oscillations (Kiessig fringes) in the off-specular scatterings signifies a high degree of structural vertical correlation from layer to layer with a vertical correlation length larger than the total ML thickness [12,22]. Thus, the spatial roughness pattern in successive layers is replicated from the substrate upwards to the top layers.

Rocking curves and their fits are plotted in Figure 3b. Several basic models for the roughness cross-correlation within a ML have been reported in the literature and are discussed in detail in reference [12]. The models are developed based on the different possibilities of roughness correlation along the ML structure. The model of Holý and Baumbach [22] assumes complete correlation. It takes into account that interfaces are formed successively from the substrate to the surface. Each interface adds some statistically independent roughness, which is assumed to be completely transferred to all subsequent interfaces. We found the best agreement with this model for our structures confirming the increase in roughness. Thus, roughness is accumulated, and σ increases with N. The fitting parameters are σ, the fractal dimension h, and the lateral correlation length ξ. The vertical correlation length κ is found to be

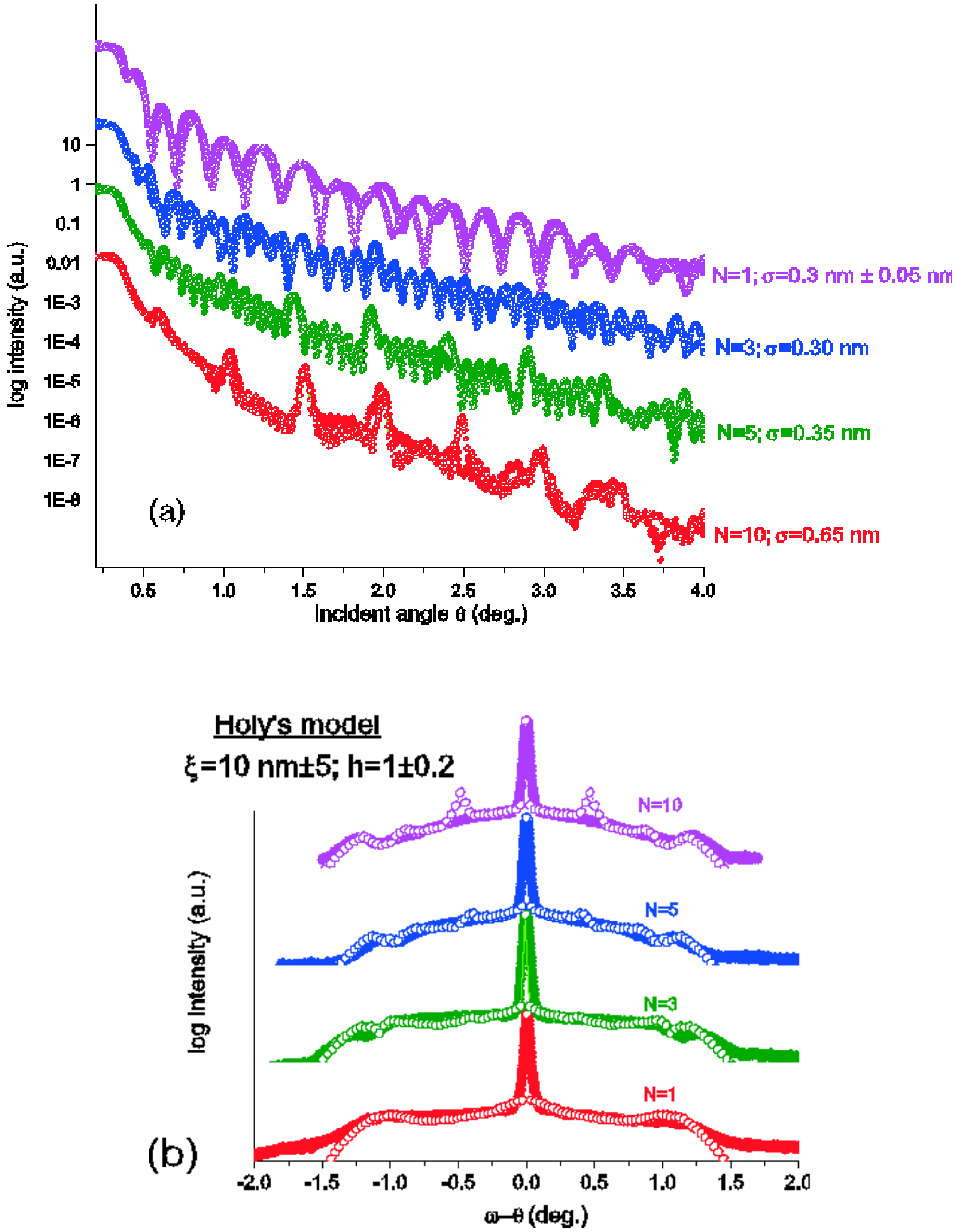

Fig. 3. (a) Specular and (b) off-specular X-ray scattering of SiO_2/NiFe(10.0 nm)/[IrMn(6.0 nm)/CoFe(3.0 nm)] × N ML. Filled symbols are the data and open symbols the fits.

larger than the total ML thickness. We observe no significant dependence of h and ξ on N. Typical uncertainties of ξ and h are ± 5 nm and ± 0.2, respectively. The texture of the multilayeres were investigated by X-ray diffraction technique (XRD) and was found similar for all N.

An increase in $\sigma_{interface}$ may increase the number of uncompensated pinned spins. Theoretical models have suggested that the mechanism of exchange coupling is related to uncompensated spins at domains walls [23]. Films with large domains necessarily have a low domain wall density and hence only few uncompensated spins. However, Liu et al. [24] have shown that a roughness increase of around 0.6 nm associated with a in-plane variation of correlation lengths by $\sim$30 nm can cause the H_{EB} to increase by only 50 Oe for NiFe/FeMn based systems. Whereas for systems where the correlation length is larger than the grain size no increase in H_{EB} was found. In the present case the interface roughness change is only 0.3 nm with no variation in the very small lateral correlation length. We believe that the small increase of $\sigma_{interface}$ is not responsible for the observed increase of H_{EB} with N, because the accompanying small variation in the number of

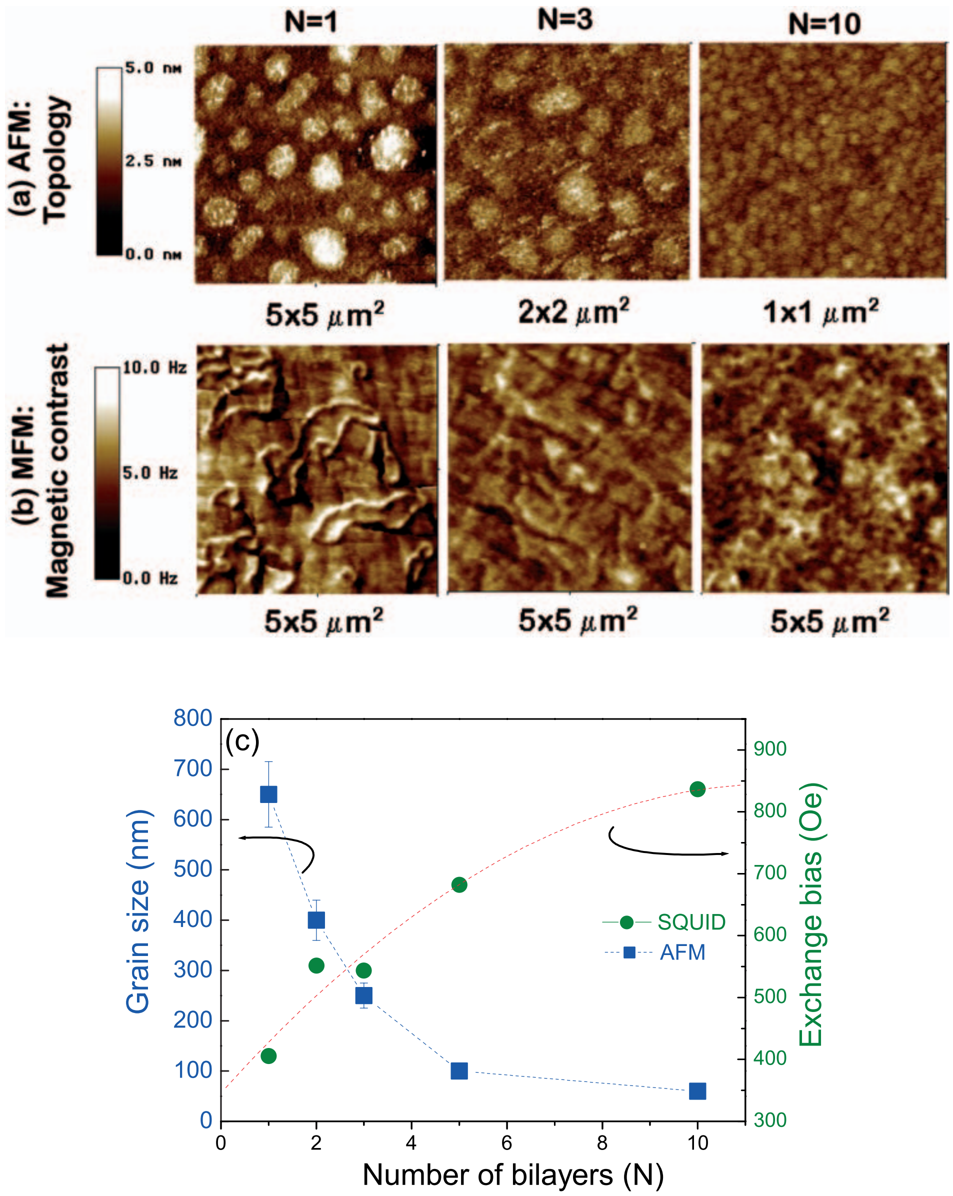

Fig. 4. (a) AFM and (b) MFM micrographs of SiO_2/NiFe(10.0 nm)/[IrMn(6.0 nm)/CoFe(3.0 nm)]$_N$ MLs. MFM images are recorded at zero field after saturating the specimens in the field-cooling direction. Note the different image sizes in (a). (c) Correlation of the dependencies of the grain size and H_{EB} on N. Dashed lines are guides to the eyes.

uncompensated spins due to roughness at the interface is not sufficient to explain the large variation of H_{EB}.

3.3 Scanning probe microscopy

Microstructural analysis by AFM shown in Figure 4a, however reveal a variation in grain size that has decreased from 650 nm for $N = 1$ to 60 nm for $N = 10$ [Fig. 4c]. Moreover, the MFM micrographs [Fig. 4b] indicate a significant change of the magnetic domain structure with N: The extended domains for $N = 1$ gradually form structures of about 500 nm in diameter for $N = 10$.

We attribute the enhanced H_{EB} to the 10-fold shrinking of the grain size, rather than to the small increase of σ by only 0.3 nm. Due to the absence of long-range dipolar interactions in an AF, domains are stabilized by energetically preferred sites such as grain boundaries [25]. Therefore, we explain the enhancement of H_{EB} in the framework of the domain-state model for exchange bias [26,27]. The smaller grain size at larger N gives rise to smaller AF domains and, thus, a higher density of uncompensated spins, which are aligned during field-cooling and then couple to the FM layer [27,28]. The shrinking of the FM domains with increasing N confirms a link between the grain size and the magnetic ordering. However, we cannot directly correlate AF domains with the observed FM domains as in reference [29], because our samples are field-cooled.

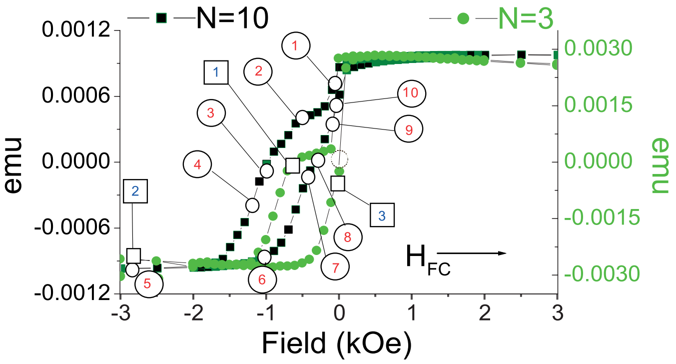

Fig. 5. Magnetization loop of SiO_2/NiFe(10.0 nm)/[IrMn(6.0 nm)/CoFe(3.0 nm)]$_{10}$. Open numbered circles and squares mark the locations of the PNR measurement along the loops for $N = 10$ and 3, respectively. The dotted circle is the reversal point of the increasing field branch of the $N = 3$ loop at about $H_a = -10$ Oe.

3.4 Neutron measurements

We perform PNR measurements for two MLs with different N. This means they have different grain sizes of 60 nm ($N = 10$) and 250 nm ($N = 3$). Measurements are done at 15 and 7 different fields H_a applied collinear to H_{FC} on both sides of the hysteresis loop for both MLs in order to study the layer-resolved magnetization state and reversal behavior. Figure 5 shows the representative fields in circled numbers for neutron measurements. Figures 6 and 7 show the respective NSF (R_{++}) and SF intensity (R_{+-}) maps as a function of α_i and α_f for $N = 10$, whereas Figure 8 shows the SF intensity (R_{+-}) maps for $N = 3$ at different representative fields H_a [see circled numbers in Fig. 5].

3.4.1 Off-specular scattering

ML with N = 10

Off-specular intensity in the SF channel appears near the critical angle $\alpha_c \approx 4$ mrad in panels ③, ④, and ⑦, ⑧, ⑨, ⑩ i.e. in both loop branches near the reversal, but not in the saturated state at $H_a = -2.8$ kOe in panel ⑤. This is a clear difference to the data in reference [9] and indicates that the off-specular intensity is related to the reversal process rather than to magnetic disorder due to, for instance, interface roughness. The off-specular scattering is most intense at the two fields where the net magnetization of the ML vanishes (reversal point) [panel ③ and ⑧] and gradually diminishes [e.g. panel ⑤] to disappear in saturation.

In the NSF channel however, a very weak Bragg sheet intensity is seen for $H_a = 2.8$ kOe or the saturated state which is due to the conformal interface roughness. We also find NSF off-specular intensities around $\alpha_c \approx 4$ mrad which is weaker than that found in SF channels at the respective reversal fields (increasing/decreasing) which arises from small fluctuations along the field.

ML with N = 3

Off-specular SF intensity also appears for $N = 3$ ML (Fig. 8) near the critical angle $\alpha_c \approx 4$ mrad in both loop branches near the reversal point [panel ② and ④], but not in the saturated state at $H_a = -2.8$ kOe [panel ③]. The off-specular scattering is most intense at the field at the reversal point where $H_a = -600$ Oe for decreasing field [panel ②] and gradually diminishes to disappear in saturation [panel ③], before it starts to appear again for increasing field at $H_a = -50$ Oe [panel ④]. The reversal and the vanishing of the net magnetization for the increasing branch occurs at about −10 Oe (dotted circle in Fig. 5), but we cannot measure at an applied field lower than −50 Oe [panel ③] without depolarizing the neutron beam.

We now refer to Figure 7 for comparison the SF intensity (R_{+-}) maps from the ML with $N = 10$ for the increasing branch at $H_a = -400$ and -300 Oe [panel ⑦ and panel ⑧]. In this case, due to the stronger exchange bias effect, we can reach the reversal point at $H_a = -300$ Oe. We now compare the map of the state before reaching the reversal point for $N = 10$ at $H_a = -400$ Oe [panel ⑦ in Fig. 7] with the state for $N = 3$ at $H_a = -50$ Oe [panel ④ Fig. 8]. In both cases, we observe the appearance of off-specular scattering close to the magnetization reversal processes.

The presence of off-specular SF intensity (in both MLs) confirms that the in-plane magnetization component perpendicular to the guiding field $M_\perp$ is laterally inhomogeneous on a length scale smaller than $l_\parallel$. The fact that the off-specular intensity extends to $\alpha_i = \alpha_c$ and $\alpha_f = \alpha_c$ implies that the inhomogeneities occur on a length scale clearly below 1 μm [30]. The high intensity at α_c arises from the enhanced transmission coefficient at the critical angle and is not related to a length scale. Thus, we think of the inhomogeneities as fluctuations of $M_\perp$ rather than magnetic domains. When the domain sizes are small and is comparable with the domain wall width it is reasonable to think of such small scale variations across the domain wall as fluctuations just before they flip with the field. A quantitative evaluation of the lateral length scale is beyond the scope of the present measurement geometry. The absence of off-specular intensity in the Bragg sheets signifies that there is no correlation of the $M_\perp$ fluctuations along the thickness of the sample. The length scale of these fluctuations (below 1 μm) and the grain sizes supports the idea that domain walls at the grain boundaries give rise to excess magnetization in the AF. To our knowledge, this is the first ever observation of such magnetization fluctuations which are directly linked to the magnetization reversal of exchange biased systems from vertically uncorrelated magnetic domains. Earlier Marrows et al. reported [31] on multilayered structures with vertically correlated domains.

We show a qualitative simulation for the SF specular and off-specular intensity in Figure 9 for $N = 10$ corresponding to $H_a = -50$ Oe on the decreasing branch considering (a) without and (b) with vertical correlation.

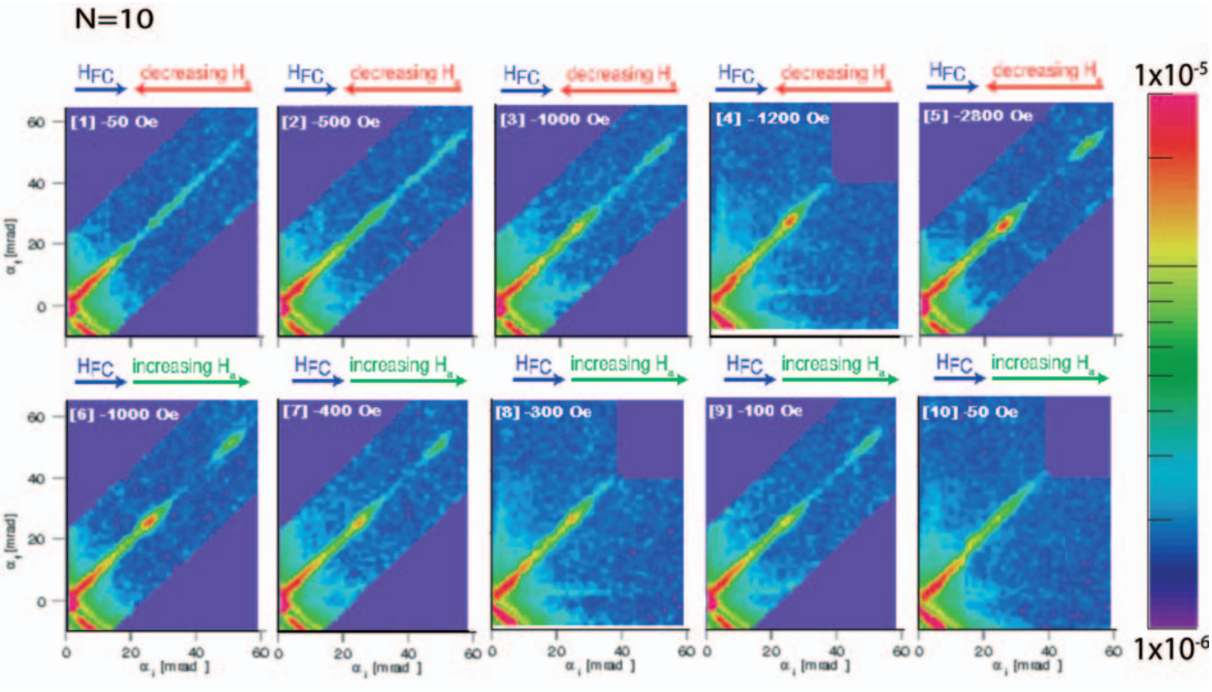

Fig. 6. NSF reflectivity maps R_{++} of a SiO$_2$/NiFe(10.0 nm)/[IrMn(6.0 nm)/CoFe(3.0 nm)]$_{10}$ ML at different positions along the magnetization loop [see Fig. 5]. Off-specular intensity appears near the switching for both decreasing [② to ④] and increasing [⑦ to ⑩] loop branches but is absent in the saturated state ⑤.

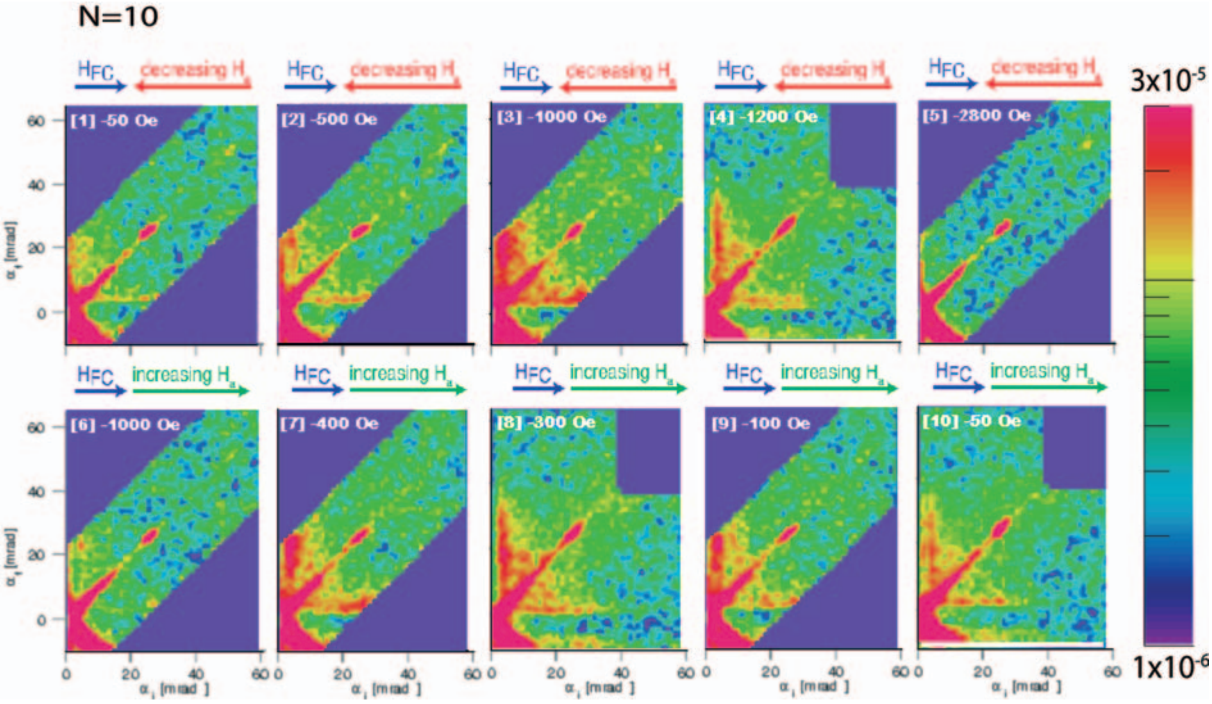

Fig. 7. SF reflectivity maps R_{+-} of a SiO$_2$/NiFe(10.0 nm)/[IrMn(6.0 nm)/CoFe(3.0 nm)]$_{10}$ ML at different positions along the magnetization loop [see Fig. 5]. Off-specular intensity appears near the switching for both decreasing [② to ④] and increasing [⑦ to ⑩] loop branches but is absent in the saturated state ⑤.

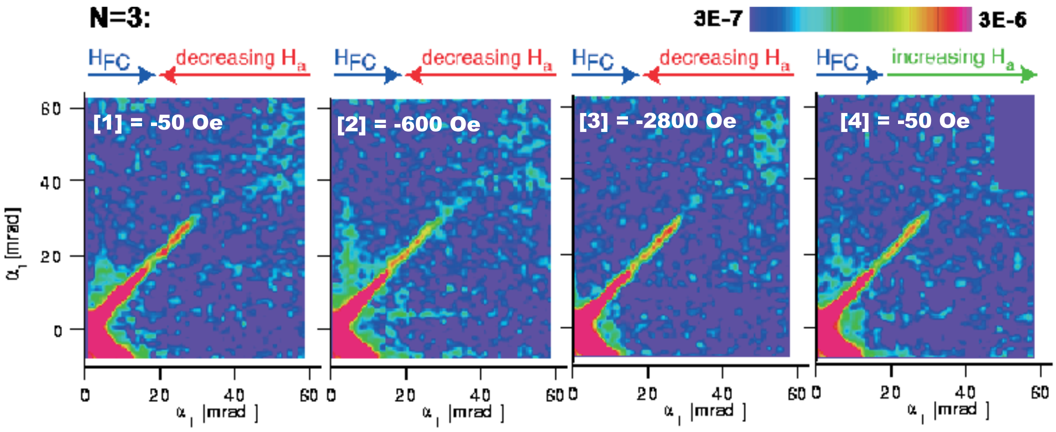

Fig. 8. SF reflectivity maps R_{+-} of a SiO$_2$/NiFe(10.0 nm)/[IrMn(6.0 nm)/CoFe(3.0 nm)]$_3$ ML at different positions along the magnetization loop [see Fig. 5]. Off-specular intensity appears near the switching for both decreasing [②] and increasing [④] loop branches but is absent in the saturated state ③.

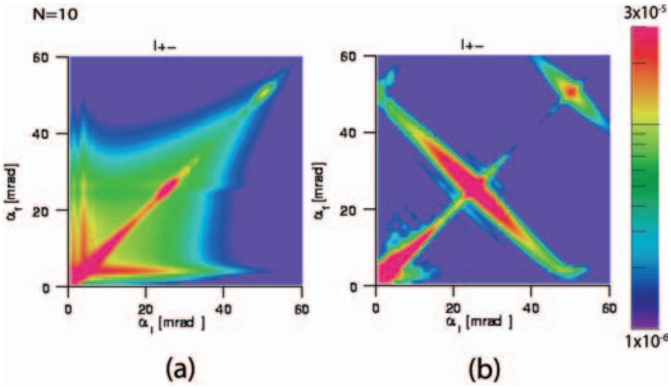

Fig. 9. Simulation for SF reflectivity maps R_{+-} of a SiO$_2$/NiFe(10.0 nm)/[IrMn(6.0 nm)/CoFe(3.0 nm)]$_{10}$ ML at $H_a = -50$ Oe on the increasing branch showing the scattering from magnetic structures (a) without and (b) with vertical correlation.

The data are simulated within the DWBA approximation [30,32] and properly take into account the limited efficiencies of the polarizer and the analyzer. Comparing the corresponding experimental data with the simulated one we conclude the absence of any vertical correlation of the magnetic domains/fluctuations along the stack. This also indicate that the ML structure is uncoupled and thus we expect layer by layer magnetometry. Magnetic roughness is expected to be highly correlated with the chemical roughness [33]. The scattering contribution from in-plane variation of magnetic roughness is much weaker over the low variation due to structural roughness in our samples. We do not observe any vertical correlation which is of magnetic origin.

3.4.2 Specular reflectivity

The specular intensity in Figures 6, 7 and 8 along the line $\alpha_i = \alpha_f$ shows first order and weak second order Bragg peaks at $\alpha_{i,f} \approx 25$ and 50 mrad corresponding to the bilayer thickness. The fitting of the specular reflectivities described below confirms that all these Bragg peaks are of NSF nature and appear in the SF channels due to the non-ideal polarization efficiencies.

All four specular reflectivity channels are measured at different H_a, among them we show eight in Figure 10 ($N = 10$) and four in Figure 11 ($N = 3$) [circled numbers refer to Fig. 5] together with least-square fits [34] based on an extension of the Paratt formalism [19] to magnetic MLs [35].

First we inspect the data. The two peaks in the NSF channels (R_{++} and R_{--}) are the first and second order Bragg reflections of the ML. The corresponding weak peaks in the SF channels (R_{+-} and R_{-+}) can be reproduced in the fits by taking into account the polarization efficiencies of our setup. R_{++} and R_{--} are much close to each other at $H_a = -1000$ Oe [②] for $N = 10$ (Fig. 10) and $H_a = -600$ Oe for $N = 3$ (Fig. 11) on the decreasing branch. Whereas reflectivities are closest at $H_a = -300$ Oe [⑤] for $N = 10$ on the increasing branch. This signify that the reversal for both loop branches proceeds via a state with an almost vanishing magnetization component collinear to H_a. For all other fields R_{++} or R_{--} are with higher intensities and reflects a net magnetization collinear with H_a, while the specular SF intensities are always much weaker.

We continue discussing the reflectivity patterns where we observe magnetization reversal along both the branches of hysteresis loop. In Figure 12a we show the measured specular SF intensity for $\alpha_{i,f} = \alpha_c$ as a function of H_a and compare with the calculated specular SF intensity for the situation where the full ML magnetizations are aligned perpendicular to H_a (dashed line). Obviously, the data indicates a much smaller $M_\perp$. In a next step, we calculate the specular SF intensity under the assumption that the magnetization of only one CoFe layer is perpendicular to H_a and all others collinear to H_a. The resulting specular SF intensity depends on which layer along the stack we choose to be perpendicularly magnetized. The range of values is marked in Figure 12a by the grey region. We

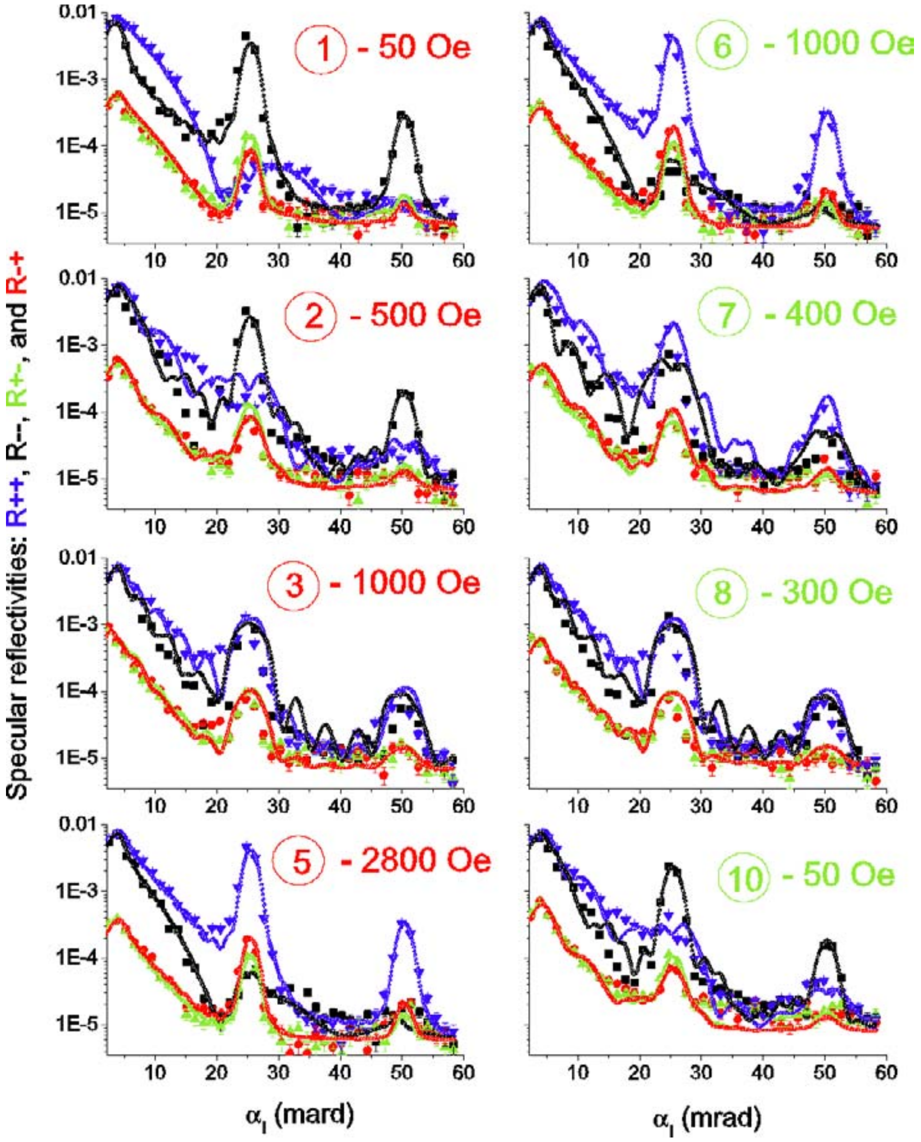

Fig. 10. Specular reflectivities R_{++} (blue), R_{--} (black), R_{+-} (green), and R_{-+} (red) of a SiO_2/NiFe(10.0 nm)/[IrMn(6.0 nm)/CoFe(3.0 nm)$]_{10}$ at different positions along the magnetization loop [circled numbers refer to Fig. 5]. Filled symbols are the data and open symbols the fits.

conclude from these comparisons, that the magnetization reversals in both directions do not proceed via magnetization rotation, neither of all layers together nor of one at a time.

For a more quantitative analysis, we first fit the specular intensities in the saturated state [⑧ in Fig. 10 and ④ in Fig. 11] to adjust the nuclear and magnetic scattering length densities, the layer thicknesses, and the interface roughness. We find excellent agreement with the XRR data for the thicknesses and the roughness and keep them as well as the nuclear scattering length densities fixed for all subsequent fits. For the non-saturated states we have to vary the magnetization configuration of the ML, which – in principle– requires to introduce a magnetization amplitude M_i and direction θ_i ($i = 1 \ldots 10$) for each CoFe layer. Based on the conclusions from Figure 12a we can reduce the number of fitting parameter by only considering configurations where each CoFe layer is roughly aligned either parallel or antiparallel to H_a. Deviations from the purely collinear, single domain configurations (i.e. $\theta_i = 0$ or 180 degree, M_i equal to the saturation magnetization of CoFe for all i) are described by the mean magnetization amplitude $M = \langle M_i \rangle$ and the mean angular deviation from the collinear alignment $\Delta\theta = \langle \Delta\theta_i \rangle$ averaged over all CoFe layers $i = 1 \ldots 10$. In this way the number of fitting parameters is kept manageable. We fit the data for all permutations of collinear configurations in order to identify the configuration yielding the best agreement between fit and data. The results are shown in Figure 12b: For decreasing H_a the CoFe layers switch sequentially from the

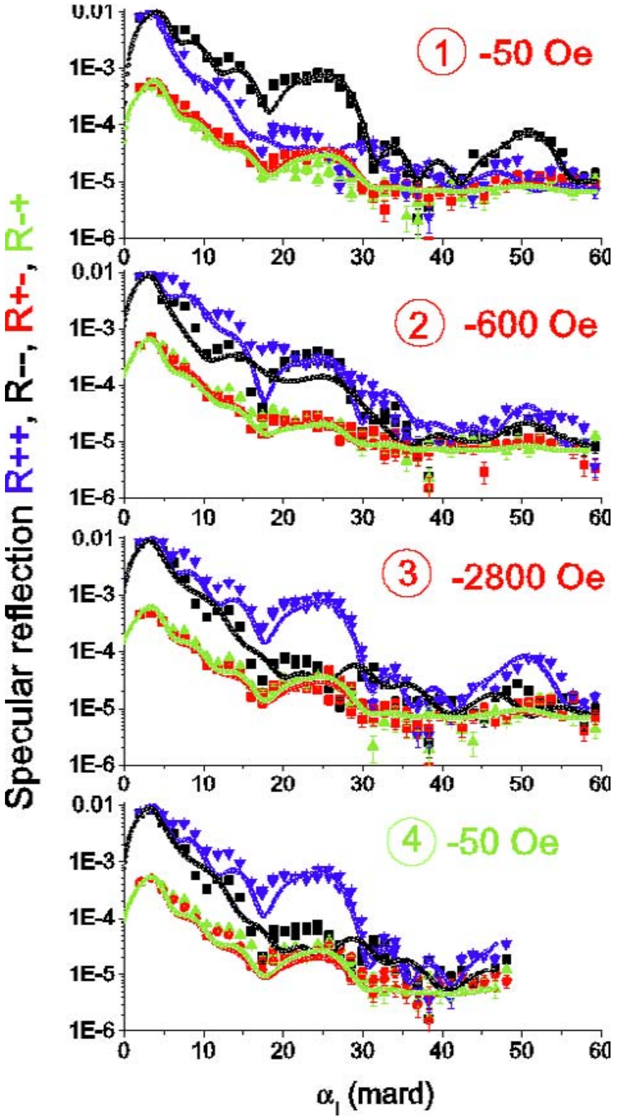

Fig. 11. Specular reflectivities R_{++} (blue), R_{--} (black), R_{+-} (green), and R_{-+} (red) of a SiO_2/NiFe(10.0 nm)/[IrMn(6.0 nm)/CoFe(3.0 nm)]$_3$ at different positions along the magnetization loop [circled numbers refer to Fig. 5]. Filled symbols are the data and open symbols the fits.

bottom to the top, and for increasing H_a the reversal proceeds in the opposite direction. The sequential switching scheme perfectly fits in to our $N = 3$ (Fig. 11) specimen also.

This sequential switching of the layers is due to the structural evolution along the ML. The layers at the top consist of smaller grains that yield a stronger exchange bias in agreement with the data in Figure 2. Therefore, they align last with a field applied antiparallel to H_{FC}, but first when H_a is again increased. The fitted mean magnetization amplitude M does not show significant variations except for the lowest fields (–50 Oe) where it is decreased by 11% for $N = 10$. A small number of domains that form when one approaches $H_a = 0$ explain this decrease. For

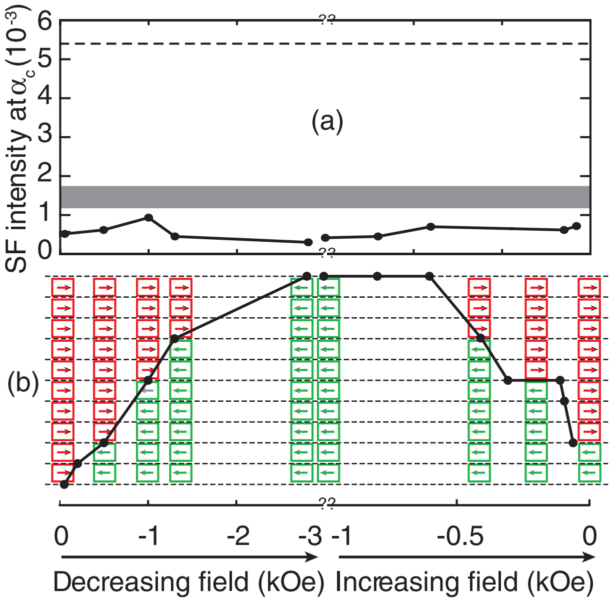

Fig. 12. (a) Experimental (symbols) and simulated (dashed line and grey region) SF intensity for $\alpha_{i,f} = \alpha_c$ as a function of H_a. The data is not compatible with perpendicular alignment of the whole ML (dashed line) nor a single CoFe layer (grey region), see text. (b) Switching sequence along the ML from the bottom to top and back as obtained from the fits. For some field values, each CoFe layer in the ML is represented box and the arrows indicate a layer magnetization parallel (red) or antiparallel (green) to H_{FC}.

$N = 3$ case M is reduced to 30–50% at the reversal point (–600 Oe). For $N = 3$ case, the number of layer flipped and which remain un-flipped cannot be equal, thus a lower net magnetization at reversal point. The mean angular deviation $\Delta\theta$ is small except for –1 kOe [②] ($N = 10$) and –600 Oe [③] ($N = 3$) on the decreasing branch, where it amounts to 8degree. This deviation is in agreement with the maximum specular and off-specular SF intensity in Figure 7.

The observation of symmetric nonuniform reversal of magnetization is different since other systems mainly show asymmetric reversal behavior. Lack of any spin-flip specular reflectivity at reversal points is strongly supported by the variation of the significant diffuse scattering with field. Lee et al. [6], indicated domain rotation based indirectly upon specular reflectivities only. We discuss below how our results contribute in developing the current understanding of exchange bias. Firstly, we our system show the reversal mode predicted by Beckmann et al. for the case without misalignment between the field cooling axis and the applied field field axis. This reversal mode – symmetric, but non-uniform – corresponds to the situation for $\theta = 0$ for our polycrystalline specimens. This was considered unlikely to occur in experiments by Beckmann et al. [11]. Secondly, we observe and simulate fluctuations of $M \perp$ at the reversal points in agreement to our experimental data for the first time which are a reflection of the state of instability occurring for the situation when the effective field acting on the FM is aligned with the applied field [11].

These fluctuations indicate a more complex reversal mechanism than hitherto considered. Thirdly, we show that the domain state model can be applied to to much wider class of systems, which can as well be polycrystalline, than realized today other than single-crystalline diluted specimens. This is seen by the fact that we observe sequential switching along the stack due to the variation in exchange bias field and we observe un-correlated domains through the ML stack. Thus the grain boundaries play the role of non-magnetic defects of the so called domain state model [27] and pin domain walls in the AF. Fourthly our samples are MLs unlike the bilayer specimens investigated experimentally [7–9] as well as theoretically [11]. MLs in our case differ from a bilayer in a sense that the pinned FM interface is pinned by the AF layer on both sides (AF-FM-AF), whereas a bilayer (FM-AF) would have only one such interface. A bilayer system is thus intrinsically asymmetric, whereas a ML is symmetric. We confirm our present observation also in another polycrystalline $[Co/CoO]_{20}$ ML where a very similar reversal mechanism by domain nucleation is seen to take place [36].

In conclusion, we observe a sequential reversal of the FM layers in a $[IrMn/CoFe]_{10}$ ML which is directly related to the evolution of the grain size along the stack. The nonuniform reversal of each CoFe layer proceeds symmetrically via domain wall motion for both remagnetization directions. Reversal by coherent magnetization rotation is excluded due to the too weak specular spin-flip intensity. However, the reversals are accompanied by fluctuations of the in-plane magnetization component perpendicular to the external field on a length scale shorter than 1 μm as directly evidenced by off-specular spin-flip PNR data. This fluctuations are observed for the first time for such vertically un-correlated domains. All our findings –the dependence of H_{EB} on N, the sequential switching, and the fluctuations at reversal– are consistent with a picture where the exchange bias is mediated by uncompensated spin at AF domain walls, which are located at grain boundaries [25]. The resulting laterally inhomogeneous interfacial exchange coupling gives rise to magnetic fluctuations at reversal. The expected length scale of the fluctuations of 10–100's of nm and the grain size (60 to 650 nm) is well compatible with our off-specular spin-flip PNR data. The reversal mechanism is similar for specimens with $N = 3$ and $N = 10$ although their grain sizes differ by a factor of about four. Therefore, a variation of the grain size –at least for grain sizes below about 1 μm– and the related AF domain size has a strong impact on the magnitude of the exchange bias effect, but does not influence the reversal mechanism.

References

1. We assume a positive direction of H_{FC} and call the field sweep from positive to negative (negative to positive) saturation the decreasing (increasing) loop branch
2. W.H. Meiklejohn, C.P. Bean, Phys. Rev. **102**, 1413 (1956)
3. B. Dieny, J. Magn. Magn. Mater. **136**, 335 (1994)
4. J. Nogués, I.K. Schuller, J. Magn. Magn. Mater. **192**, 203 (1999); A.E. Berkowitz, K. Takano, J. Magn. Magn. Mater. **200**, 552 (1999)
5. V.I. Nikitenko et al., Phys. Rev. Lett. **84**, 765 (2000)
6. W.-T. Lee et al., Phys. Rev. B **65**, 224417 (2002)
7. M.R. Fitzsimmons et al., Phys. Rev. Lett. **84**, 3986 (2000)
8. M. Gierlings et al., Phys. Rev. B **65**, 92407 (2002)
9. F. Radu et al., Phys. Rev. B **67**, 134409 (2003)
10. B.C. Choi et al., Appl. Phys. Lett. **77**, 892 (2000)
11. B. Beckmann, U. Nowak, K.D. Usadel, Phys. Rev. Lett. **91**, 187201 (2003)
12. A. Paul, G.S. Lodha, Phys. Rev. B **65**, 245416 (2002)
13. S.K. Sinha et al., Phys. Rev. B **38**, 2297 (1998)
14. T. Salditt, T.H. Metzger, J. Peisl, Phys. Rev. Lett. **73**, 2228 (1994)
15. U. Rücker et al., Physica B **276-278**, 95 (2000); U. Rücker et al., Physica B **297**, 140 (2001); for information on HADAS see: `http://www.fz-juelich.de/iff/wns_hadas`
16. J.A.C. Bland, J. Vac. Sci. Technol. A **15**, 1759 (1997)
17. C.H. Marrows, S. Langridge, B.J. Hickey, Phys. Rev. B **62**, 11340 (2000)
18. V. Lauter-Pasyuk et al., Phys. Rev. Lett. **89**, 167203 (2002)
19. L.G. Paratt, Phys. Rev. **95**, 359 (1954)
20. L. Nevot, P. Croce, Rev. Phys. Appl. **15**, 761 (1980)
21. A. Paul et al., J. Phys.: Condens. Matter **15**, 2471 (2003)
22. V. Holý, T. Baumbach, Phys. Rev. B **49**, 10668 (1994)
23. A.P. Malozemoff, Phys. Rev. B **35**, 3679 (1987)
24. C. Liu et al., J. Appl. Phys. **87**, 6644 (2000)
25. H. Ohldag et al., Phys. Rev. Lett. **91**, 017203 (2003)
26. P. Miltényi et al., Phys. Rev. Lett. **84**, 4224 (2000)
27. U. Nowak, K.D. Usadel, J. Keller, P. Miltényi, B. Beschoten, G. Güntherodt, Phys. Rev. B **66**, 14430 (2002)
28. J. Keller, P. Miltényi, B. Beschoten, G. Güntherodt, U. Nowak, K.D. Usadel, Phys. Rev. B **66**, 14431 (2002)
29. F. Nolting, A. Scholl, J. Stöhr, J.W. Seo, J. Fompeyrine, H. Siegwart, J.-P. Locquet, S. Anders, J. Lüning, E.E. Fullerton, M.F. Toney, M.R. Scheinfein, H.A. Padmore, Nature **405**, 767 (2000)
30. B.P. Toperverg, "*Polarized Neutron Reflection and Off-Specular Scattering*" in *Polarized Neutron Scattering*, edited by Th. Brückel, W. Schweika, Forschungszentrum Jülich, Series "*Matter and Materials*", Vol. 12 (2002)
31. C.H. Marrows et al., Phys. Rev. B **66**, 24437 (2002)
32. E. Kentzinger, U. Rücker, B.P. Toperverg, Physica B **335**, 82 (2003)
33. M.R. Fitzsimmons et al., J. Magn. Mag. Mater. **271**, 103 (2004)
34. J.J. Mor, *The Levenberg-Marquardt Algorithm: Implementation and Theory*, in *Numerical Analysis*, edited by G.A. Watson, Lecture Notes in Mathematics, Vol. 630 (Springer-Verlag, Berlin, 1977), pp. 105–116
35. H. Zabel, Appl. Phys. A **58**, 259 (1994); E. Kentzinger, U. Rücker, B.P. Toperverg, Physica B **335**, 82 (2003)
36. A. Paul et al. (to be published)